Smart Structures and Systems, *Vol. 34, No. 1 (2024) 41-50*
https://doi.org/10.12989/sss.2024.34.1.041

Measurement of temperature change on coil column unit using FBG sensors during thermal response test: A study for geothermal energy system

Young-Sang Kim [1a], Duc-Thang Hoang [1b], Gyeong-O Kang [2a] and Ba Huu Dinh*[1,3,4]

[1] *Department of Civil Engineering, Chonnam National University, Yongbong-ro 77, Buk-gu, Gwangju, 61186, South Korea*
[2] *Department of Civil Engineering, Gwangju University, 277 Hyodeong-ro, Nam-gu, Gwangju, South Korea*
[3] *Laboratory for Computational Civil Engineering, Institute for Computational Science and Artificial Intelligence, Van Lang University, Ho Chi Minh City, Vietnam*
[4] *Faculty of Civil Engineering, School of Technology, Van Lang University, Ho Chi Minh City, Vietnam*

(*Received May 21, 2024, Revised August 19, 2024, Accepted August 20, 2024*)

Abstract. The accurate measurement of temperature in the ground source heat pump system is crucial for assessing the thermal response of the system and validating the numerical model for parametric study, which is necessary for the thermal performance evaluation of the geothermal energy system. Conventional temperature sensors have some disadvantages such as they are difficult to install, and their position can be shifted during the backfill process of the ground heat exchanger. In this study, Fiber Bragg Grating (FBG) sensors were used to measure the temperature change of a recently developed ground heat exchanger (Coil Column Unit, CCU). FBG sensors were first calibrated in a thermal chamber alongside a correlation sensor (RTD sensor). The calibrated sensors were then mounted on the pipe surface at each spiral of the CCU to measure how temperature changes during the in-door mockup thermal response test. Finally, the measurement results of the FBG sensors were verified with a finite element coded program. The results indicated that the temperature difference between the numerical analysis and the experiment was less than 1%, which is significantly lower than that of the previous study using the RTD sensors. Therefore, it is feasible to apply FBG sensors for temperature measurement during the operation of the TRT of the geothermal energy system.

Keywords: coil column unit; FBG sensor; geothermal energy; ground heat exchanger; temperature measurement; thermal response test

1. Introduction

Facing the challenges of climate change and global warming, governments around the world have been taking drastic actions to cut greenhouse gas emissions to reach the goal of net zero Carbon by2050 (Nations, n.d.). Among the various efforts to reduce greenhouse gases, there is a need to minimize the use of fossil fuels and maximize the use of new and renewable energy. According to the REN21 report, total renewable energy demand increased by an average of 4.7% per year from 2010 to 2020, and renewable energy consumption for air conditioning in buildings in 2021 will also increase from 11.1% in 2011 to 14.2% (REN21 2023). In recent years, ground source heat pump (GSHP) systems have been widely researched and used as an energy source for heating and cooling residential and commercial buildings because of lower operating costs, and energy savings than conventional heating systems (Dinh *et al*. 2021).

A GSHP system typically consists of a heat pump system, a heat distribution system, and a ground heat exchanger (GHE). GSHP systems gain heating and cooling energy through GHE by emanating or absorbing heat from the ground, where the temperature remains reasonably constant in certain weather conditions (Marrah *et al*. 2023). Among various types of GHE used for GSHP systems, vertical GHE is widely utilized due to its high heat transfer efficiency and less effect by environmental conditions. However, the drilling cost for construction of the borehole of vertical GHE is very high leading to an increase in the total investment cost and therefore, preventing the spread use of the system. Horizontal GHE installed at a shallow depth of 1-3 m can overcome the high cost of the vertical GHE (Dinh *et al*. 2022). However, it generally requires a larger installation area owing to the low heat exchange capacity at the shallow installation depth. Therefore, many studies have been conducted to increase the heat transfer efficiency of the horizontal GHE.

To increase the performance of HGHE, recent studies use new configurations (slinky type, Spiral-coil type) to replace the traditional U-type GHE system. The purpose of using these new heat exchangers is to increase the heat exchange contact area, thereby increasing the heat exchange efficiency of the system. Chong *et al*. (2013) used numerical models to study the influencing factors (pitch, diameter, soil thermal conductivity) of the slinky-type GHE. The results show that reducing the pitch can improve the

*Corresponding author, Ph.D.,
E-mail: ba.dinhhuu@vlu.edu.vn
[a] Professor
[b] Master

ISSN: 1738-1584 (Print), 1738-1991 (Online)

heat transfer performance of the system, but also significantly increase the material (pipe) cost. In addition, they found that the thermal conductivity of the soil has the greatest influence on system performance, and the diameter of the slinky ring has a negligible influence. In another study, Wu *et al*. (2010) used a numerical model and observed that the diameter of the spring ring less than 1.0 m did not significantly affect the heat transfer performance of the heat exchanger. Yang *et al*. (2020) evaluated the heat transfer efficiency of all three types of heat exchangers (U-type, slinky, spiral-coil). They concluded that the spiral coil heat exchanger has better heat exchange efficiency than the slinky type of heat exchanger. They also found that increasing the thermal fluid inlet temperature and surface wind speed as well as reducing the distance between the spirals can significantly improve the heat exchange efficiency of the system. Congedo *et al*. (2012) built a CFD simulation model to evaluate and compare the heat transfer performance of three different GHE configurations. The results also show that the spiral coil-type horizontal heat exchanger exhibits the best heat transfer performance. In addition, they also concluded that soil thermal conductivity is the most important factor affecting the system's thermal performance (heat exchange efficiency doubles when soil thermal conductivity increases from 1 W/(mK) to 3 W/(mK)). More recently, Kim *et al*. (2023) proposed to use of a novel horizontal GHE called Coil-Column System (CCS). The CCS is fabricated as a single coil-column unit. The advantage of the CCS is that it can utilize the heat transfer capacity of the ground from the bottom to the top of the GHE trench, whereas in conventional GHE types, such as U-type, slinky-type, and spiral-coil type, heat transfer is primarily concentrated around the bottom of the GHE. The simulation results showed that the heat exchange capacity of this newly developed GHE is double, and three times higher than spiral coil type and U-type GHEs, respectively.

It should be noted that to investigate the parameter effect and design the capacity of the GHE, numerical study is utilized due to it can save the cost and time compared to that of the full-scale experiment. To ensure the reliability and accuracy of the numerical model, it should be validated with the experimental (e.g., thermal response test) by comparing the water temperature and soil temperature change during the heat transfer process. For this purpose, traditional electrical sensors such as thermal resistance detectors (RTD) and thermocouples are generally employed. However, these sensors have shortcomings such as being susceptible to electromagnetic radiation, poor long-term stability, being bulky, and extremely difficult to fix the sensor on the pipe wall during installations leading to significant differences in the temperature measurement obtained from sensors with the results obtained from the numerical model. In the study of Yang *et al*. (2020), for example, the thermocouple sensor was utilized and attached to the outer surface of each spiral of the spiral HGHE. The finding showed that the temperature measurement results from the experiment were higher than the results from the numerical model. Moreover, the temperature differences between experimental results measured by RTD sensors and numerical results obtained from the TRNSYS model presented in the study of Montagud *et al*. (2013) was 2%, in the study of Shah *et al*. (2022) was 4%, and in the study of Raab *et al*. (2005) was lower than 5%.

To overcome the disadvantages of conventional sensors (e.g. RTD sensor, thermocouple sensor), the Fiber Bragg Grating (FBG) sensor has been raised as a reliable and accurate sensor in applying for measuring temperature. Because it has many advantages such as small volume, anti-electromagnetic interference, corrosion resistance, easy remote operation, easy multiplexing, and so on (Cheng-Yu *et al*. 2016). The application of FBG sensors in measuring temperature has been paid attention to by researchers (Kumar *et al*. 2016, Li *et al*. 2022). For the application in temperature measurement of the ground heat exchanger, the FBG sensor was also utilized in the study of Chen *et al*. (2023). In this study, they aimed to develop a method for measuring the temperature distribution of the fluid inside the tube based on FBG sensors. The study highlighted the superior reliability and repeatability of FBG sensors, with variances of less than 0.2°C in a time period of 35 months compared to thermocouple sensors. Additionally, Ren *et al*. (2004) evaluated the reliability of GSHP systems by employing FBG sensors to measure temperature fluctuations along the GHE pipe. The findings concluded that FBG sensors can be applied over an extended period.

This study proposes to use FBG sensors for measuring the temperature change on each spiral of the coil-column unit (a part of coil-column system recently developed by Kim *et al*. (2023)). With the aim of improving the efficiency of heat exchanger temperature measurement methods, it is anticipated that this method could potentially replace other sensors in future temperature measurement applications. For this purpose, the FBG sensors were initially calibrated in a thermal chamber to obtain the correlation equation between the wavelength shift of the FBG sensor and temperature change. Secondly, the calibration results were then incorporated into the FBG interrogator specific to each sensor. These sensors were then mounted on the pipe surface at each spiral of the CCU to measure how temperature changes during the thermal response test. Finally, the results obtained from the experiment were compared to the results obtained from the COMSOL Multiphysics model of CCU.

2. Operating principle of FBG sensor

Fiber Bragg Grating (FBG) is an optical component fabricated by precisely modulating the refractive index within the core of a single-mode fiber at periodic intervals (Wang *et al*. 2014). This modulation enables FBG to exhibit the distinctive property of selectively reflecting a narrow spectral band of incident wideband light, wherein the reflection center is carefully chosen.

When a broadband light signal is transmitted through the FBG, the incident light interacts with this periodic refractive variation (Kersey *et al*. 1997). As a result, the light is selectively reflected at a specific wavelength known as Bragg wavelength (λ_B) and it can be calculated as Lee *et al*. (2006)

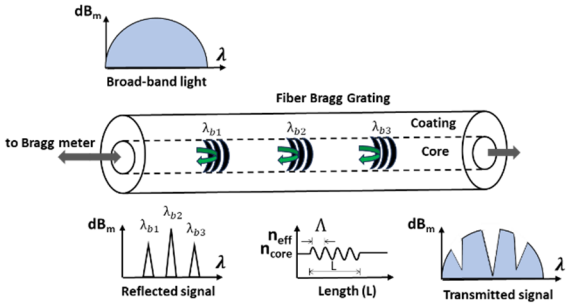

Fig. 1 General measurement scheme of FBG (Venkatesan and Ramalingam 2017)

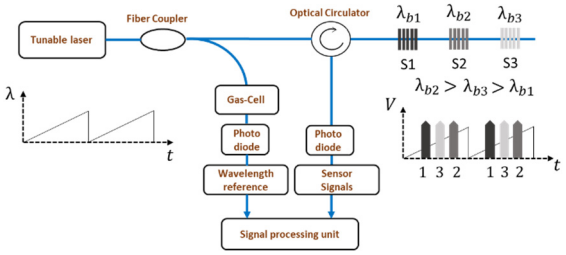

Fig. 2 Signal detection scheme (Bharathwaj *et al*. 2014)

$$\lambda_B = 2 \times n_{eff} \times \Lambda \tag{1}$$

where n_{eff} is the effective refractive index of the fiber core and Λ is the grating period. Fig. 1 illustrates an FBG sensor array achieved through the Wavelengths Division Multiplexing scheme. This array comprises a single fiber with gratings of varying periods that have been fabricated at different positions along its length.

The reflected wavelength of each sensor is subject to variation due to even the slightest perturbation of the temperature on the surface of the coil column ground heat exchange pipe. These changes in the reflected wavelength are subsequently captured and monitored utilizing the signal detection scheme illustrated in Fig. 2.

Typically, the impact arising from strain is much higher than the impact arising from temperature without any packaging. Consequently, the FBG sensor's external structure is enveloped by a stainless-steel tube to reduce the unwanted influence of pre-existing deformation and significantly enhance thermal sensitivity. Upon calibration of the reflection wavelengths at various temperatures for an FBG in its unstrained state, it becomes applicable for temperature measurements.

The effects on the temperature measurement are the effect of thermal expansion and the effect of thermos-optic. The result of the partial derivative with respect to temperature of Eq. (1), is described as following Eq. (2) (Werneck 2013).

$$\Delta\lambda_B = 2 \times \left(n_{eff} \frac{d\Lambda}{dT} + \Lambda \frac{dn_{eff}}{dT} \right) \Delta T \tag{2}$$

Substituting with Eq. (2), the Eq. (3) can be rearranged as follows

$$\frac{\Delta\lambda_B}{\lambda_B} = \left(\frac{1}{\Lambda}\frac{d\Lambda}{dT} + \frac{1}{n_{eff}}\frac{dn_{eff}}{dT} \right) \Delta T \tag{3}$$

where the change in the grating period caused by the effect of thermal expansion, $d\Lambda$ is expressed as follows (Jing and Yongqian 2009)

$$d\Lambda = \alpha \times \Lambda \times dT \tag{4}$$

The change of effective refractive index caused by the effect of thermo-optic dn_{eff} can be described as follows (Jing and Yongqian 2009)

$$dn_{eff} = \zeta \times n_{eff} \times dT \tag{5}$$

The temperature sensitivity index of the fiber grating can be explained by Eq. (6) (Jing and Yongqian 2009).

$$K_T = \alpha + \zeta \tag{6}$$

where α the coefficient of thermal expansion ($°C^{-1}$), and ζ is the coefficient of thermo-optic ($°C^{-1}$). The temperature sensitivity index in Eq. (6) can be calculated as Eq. (7).

$$K_T = \frac{\Delta\lambda_B}{\lambda_B . \Delta T} \tag{7}$$

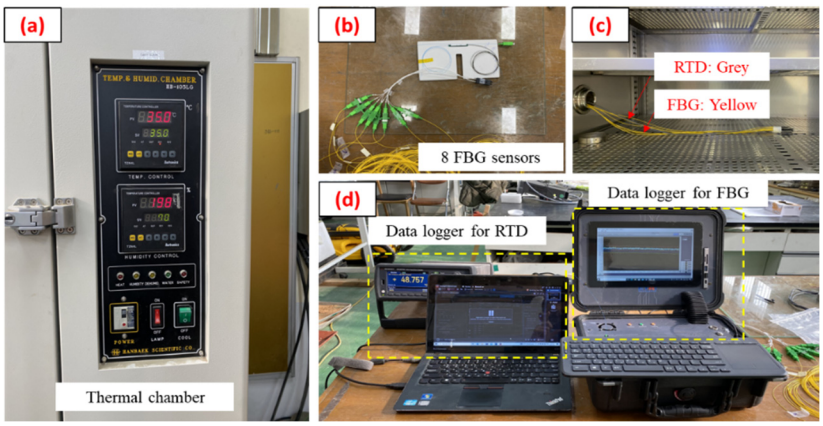

Fig. 3 Scheme of sensor calibration (a) thermal chamber; (b) FBG sensors; (c) Location of the RTD and FBG sensors inside the thermal chamber; (d) data logger for RTD and FBG sensors

where $\Delta\lambda_B/\Delta T$ is the wavelength shift with temperature nm/°C.

3. Experimental program

3.1 Calibration for FBG sensors

FBG sensors are optical sensors that use a segment of optical fiber to detect changes in temperature, strain, or other physical parameters (Talebinejad *et al*. 2009, Zhang *et al*. 2014, Kim *et al*. 2017). Calibration of an FBG sensor involves determining the relationship between the optical signal (i.e., the reflected wavelength) and the physical parameter being measured (e.g., temperature or strain) (Jing and Yongqian 2009). The calibration process involves subjecting the sensor to known physical conditions and measuring the resulting reflected wavelength. By analysing the changes in the reflected wavelength under known conditions, a calibration curve can be developed that relates the measured wavelength to the corresponding physical parameter.

In this study, a total of eight FBG sensors based on the number of the spiral of the coil column unit (CCU) shown in Fig. 3(b), were calibrated with a resistance temperature detector (RTD) sensor in a thermal chamber (Figs. 3(a)-(c)). The RTD sensors used were PT 100 (class A, accuracy of 0.15+0.002T °C).

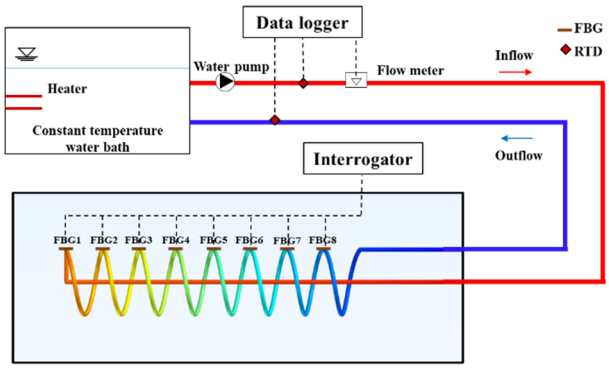

Fig. 4 Signal detection scheme

Firstly, 8 FBG sensors were connected with an optical coupler to split the input signal from the fiber optic line into multiple output channels (Fig. 3(b)). The use of an optical coupler reduces the number of fiber optic lines required to connect each sensor, making it more cost-effective and space-efficient. In addition, it allows for simultaneous measurement of multiple sensors and remote sensing in harsh environments where access to sensors is difficult or dangerous. Afterward, the coupler was connected to an FBG interrogator, as shown in Fig. 3(d). The FBG interrogator was used to measure the reflected optical signals from FBGs and extract the information encoded in them. By analyzing these parameters, the interrogator can determine the FBG's properties, such as its center wavelength, reflectivity, and bandwidth. These properties can be used to infer various physical parameters such as strain, temperature, pressure, and vibration depending on the application.

Secondly, an RTD sensor was connected to the RTD data logger to determine the temperature change as shown in Fig. 3(d). The eight FBG sensors and an RTD sensor were put in the middle space of the thermal chamber as shown in Fig. 3(c), with adjustable temperature ranges from 35°C to 60°C. To ensure suitable temperature control, it is recommended to maintain stability at 5°C increments for 20 minutes before proceeding to the subsequent level. This approach allows for sufficient time to establish a consistent temperature before progressing to the next stage. Finally, the results of the difference in temperature and associated wavelength shifts were analyzed through the use of a data logger integrated with RTD and an interrogator linked with FBG sensors, respectively.

3.2 Heat transfer in coil column unit in laboratory

To explore the experimental thermal performance of the coil column unit (CCU), an indoor thermal response test (TRT) was performed. Fig. 4 depicts the experimental setup including a mock-up steel box, a thermal response device comprising a circulating pump, a flowmeter, a single CCU, and a data acquisition system for sensors. Fig. 5 describes the experiment in the laboratory with a tank made from durable steel, possessing dimensions of 2000 × 1000 × 1000 (length × width × height) mm, and was filled with sand.

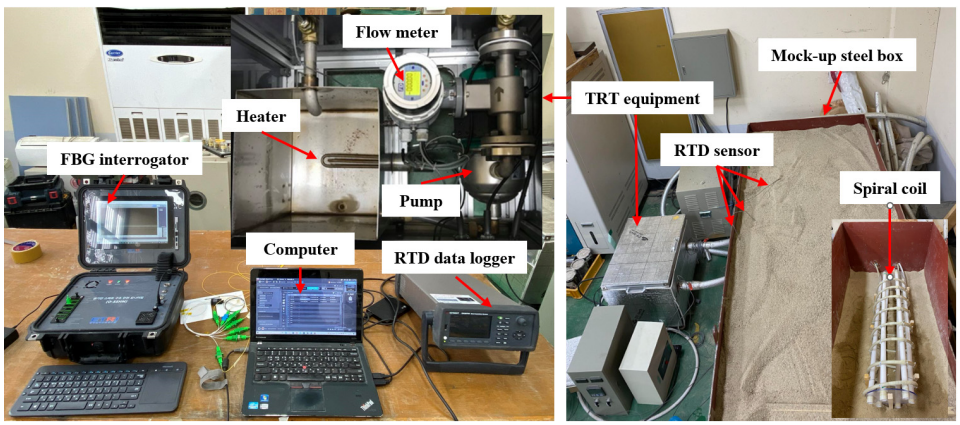

Fig. 5 TRT setup and devices

Table 1 Thermal properties of sand used in the experiment

Material	Thermal Conductivity ($W.m^{-1}. K^{-1}$)	Density ($kg.m^{-3}$)	Heat capacity ($MJ.m^{-3}. K^{-1}$)	Thermal diffusivity ($mm^2.s^{-1}$)
Sand	0.289	1786	1.273	0.198

Table 2 Equipment for TRT

Name, ID	Specification
Pump	• Wilo MHI203 M • Maximum head: 48m, rated power: 0.75 kW, maximum volumetric flow rate: 6.2 m^3/h.
Flowmeter	• FD-ATM, H, E (FD digital) • Output: DC current (4-20 mA), measurement range: 0.03-15 m/s, accuracy: ±1.0%.
Water tank	• Stainless steel water tank with a volume of 20 L.
Temperature sensors	• RTD 4 wire (PT100, Class A) • FBG sensor
Data logger	• Keysight DAQ970A • A data logger was used to record the inlet and outlet temperature measurement data flowmeter.
Data acquisition system	• DAQM901A • 20 Channel Multiplexer + 2 Channels for dedicated current measurement • Two- and four-wire scanning
PID	• Controller

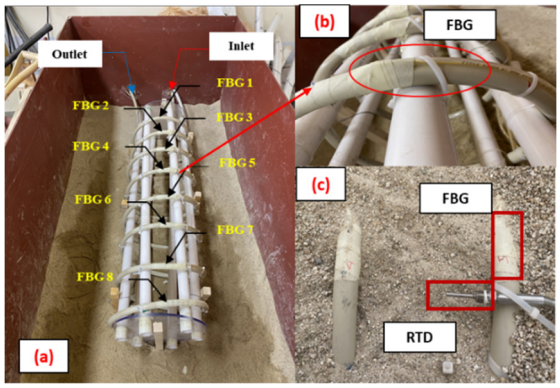

Fig. 6 Layout of FBG sensors on coil column unit

The thermal properties of the natural sand used in this experiment are presented in Table 1. The CCU was manufactured from polybutylene pipe material with an outer diameter of 20 mm and an inner diameter of 16 mm. The diameter and the pitch of the spiral coil are 300 and 150 mm, respectively, and the height of the CCU was designed at 1300 mm to fit with the dimensions of the mock-up steel box. Fluid is pumped from a pump (Wilo MHI203) that is connected to a flowmeter (FD-AMT, H, E) with a flow rate of 7.5 l/min. The fluid then proceeded to pass through the CCU, wherein the FBG sensors were positioned at each spiral location. During the thermal response test, the inlet temperature and outlet temperature were recorded by RTD sensors (PT100, 4 wire). The test equipment is reported in Table 2.

To quantify the temperature distribution along each spiral of the CCU during the heat transfer test, a total of eight FBG sensors pre-calibrated for accuracy were affixed to the external pipe of the CCU as shown in Fig. 6(a). These FBG sensors were utilized to record and obtain temperature readings of the water flowing through the CCU and protected by plastic tubes to avoid impacts during the experiment as shown in Fig. 6(b). Furthermore, three RTD sensors were strategically positioned, as depicted in Fig. 6(c), to measure the temperature of the soil during the TRT.

4. Numerical analysis

For the numerical modeling, the COMSOL Multiphysics software (Multiphysics 2015) was employed to construct a three-dimensional (3-D) domain simulating the CCU (Fig. 7). Heat transfer in the ground heat exchanger involves two primary mechanisms: the conduction of heat through the solid medium, including the soil, backfill material, and pipe wall, and the convective heat transfer of the fluid. The energy equation for the solid medium in a ground heat exchanger (GHE) can be expressed as follows

$$\frac{\partial T}{\partial t} = \alpha_s \nabla^2 T + \frac{Q}{p_s C_s} \tag{8}$$

where, t represents time in seconds (s), T denotes the temperature of the soil in Kelvin (K), and α_s is defined as the thermal diffusivity of the soil in square meters per second (m^2/s). This thermal diffusivity can be elucidated as

$$\alpha_s = \frac{\lambda_s}{p_s C_s} \tag{9}$$

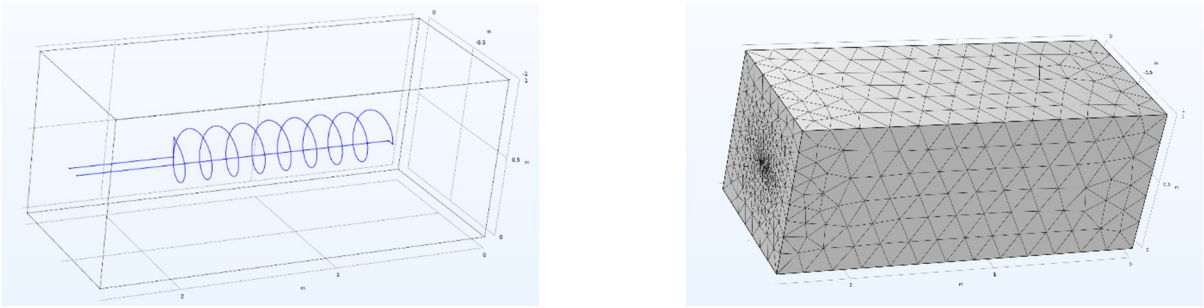

Fig. 7 Numerical models for coil column unit in the laboratory

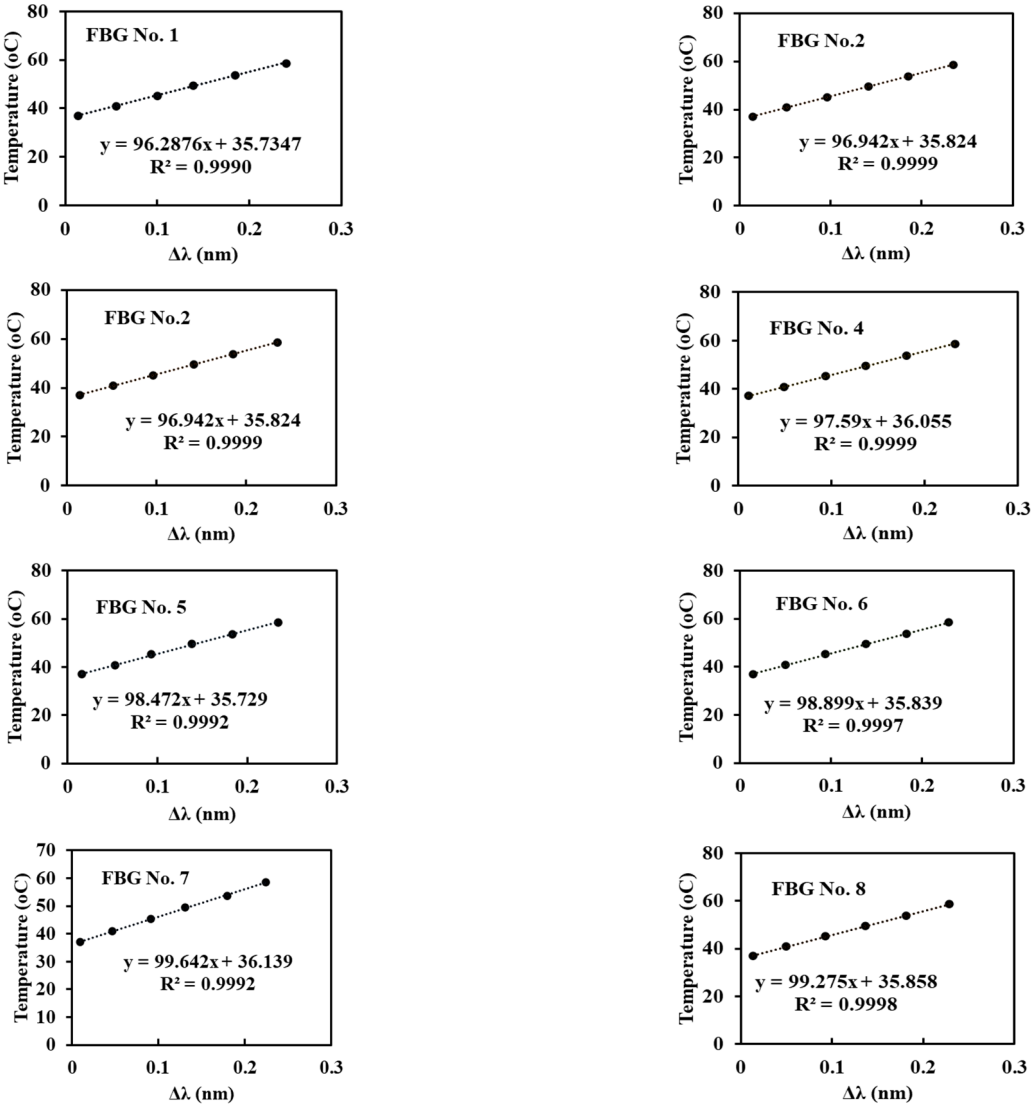

Fig. 8 The relationship between temperature and wavelength shifts of the FBG sensors

where, p_s corresponds to the density of the soil in kilograms per cubic meter (kg/m³), λ_s represents the thermal conductivity of the soil in watts per meter-kelvin (W/ (mK)), and C_s stands for the specific heat of the soil in joules per kilogram-kelvin (J/(kg.K)).

The equation for fluid energy transfer in the CCU can be described as follows (Multiphysics 2015, Dinh *et al*. 2023)

$$p_s A_p C_p \frac{\partial T_f}{\partial t} + p_f A_p C_p u.\nabla T_f = \nabla.\left(\lambda_f A_p \nabla T_f\right) + \frac{1}{2} f_D \frac{p A_p}{2 d_h} |u| u^2 + Q + Q_p \quad (10)$$

where, p_f stands for the fluid density in kilograms per cubic meter (kg/m³), T_f represents the fluid temperature in Kelvin (K), C_p is the specific heat of the fluid in joules per kilogram-kelvin (J.kg^{-1}.K^{-1}), λ_f denotes the thermal conductivity of the fluid in watts per meter-kelvin (W.m^{-1}.K^{-1}), A_p is the area of the pipe section in square meters (m²), and $f_D(pA_p/2d_h)|u|u^2$ characterizes the distribution of frictional heat dissipation due to viscosity, f_D is the friction coefficient and Churchill's equation model can be used to calculate f_D (Churchill 1977)

$$f_D = 8\left[\left(\frac{8}{Re}\right)^{12} + (C_A + C_B)^{-1.5}\right]^{\frac{1}{12}} \quad (11)$$

(Re = Reynolds number)

$$C_A = \left[-2.457 ln\left(\left(\frac{7}{Re}\right)^{0.9} + 0.27\left(\frac{e_s}{d_h}\right)\right)\right]^{16} \quad (12)$$

(e_s = surface roughness)

$$C_B = \left(\frac{37530}{Re}\right)^{16} \quad (13)$$

where d_h represents the mean hydraulic diameter in meters (m), u is the fluid velocity in meters per second (m.s^{-1}), and Q_p is the external heat exchange occurring through the pipe wall in watts per meter (W.m^{-1}).

$$Q_p = (hZ)_{eff}(T_p - T_f) \quad (14)$$

where, T_p represents the temperature of the pipe wall in Kelvin (K), T_f is water temperature, and $(hZ)_{eff}$ (W.m^{-1}.K^{-1}) denotes the relative convective heat transfer coefficient, which can be determined using the following equation (Eq. (20))

$$hZ_{eff} = \frac{1}{\frac{1}{\pi d_{in} h_{ci}} + \frac{1}{2\pi\lambda_p} ln\frac{d_{out}}{d_{in}}} \quad (15)$$

where, d_{in} and d_{out} refer to the inner and outer radius of the coiled pipe in meters (m), respectively. Additionally, λ_p represents the thermal conductivity of the pipe in watts per meter-kelvin (W.m^{-1}.K^{-1}), and h_{ci} denotes the convective heat transfer coefficient inside the pipe in watts per square meter-kelvin (W.m^{-2}.K^{-1}).

The thermal properties of the material used in the model are listed in Table 3. The inlet fluid temperature obtained from the TRT was used as the input data. In addition, the initial temperature of the sand was initialized at 12.5°C, while the boundary temperature was kept constant at 15°C (Dirichlet boundary condition), as the room temperature was set during the TRT.

5. Results and discussion

5.1 Calibration results of the Fiber Bragg Grating sensor

Fig. 8 presents the relationship between temperature and wavelengths of the FBG sensors. The coefficient of the linear association exceeds 0.9990 for all 8 sensors, indicating a highly precise and reliable correlation between temperature variation and the corresponding wavelength shifts in the FBG sensors. This calibration assessment demonstrates the robustness and accuracy of the measurement system, reinforcing its efficacy in temperature measurement applications. The correlation formula between temperature and wavelength shift $\Delta\lambda$ was then inputted into the FBG interrogator device for each FBG sensor, respectively, to continue conducting TRT of the CCU in the laboratory.

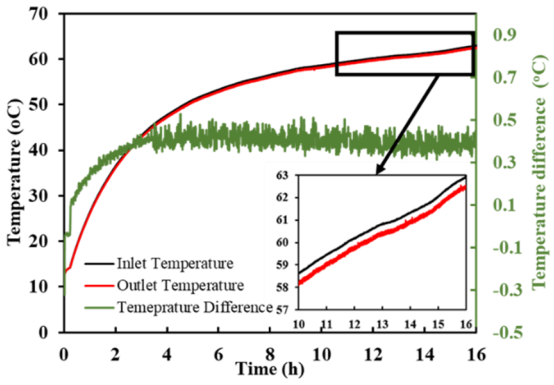

Fig. 9 Inlet and outlet temperature of the coil column unit

Table 3 Thermal properties of the material used for the numerical model

Materials	Density, (kg/m^3)	Specific heat capacity, J/(kgK)	Thermal conductivity, W/(mK)
Sand	1786	713	0.289
Circulating fluid	1000	4180	0.58
Polybutylene pipe	955	525	0.38

5.2 Heat transfer test results

Fig. 9 shows the inlet and outlet temperatures of the CCU filled with sand. In the initial 4 hours of operation, there was a swift rise in the temperature difference and reached a constant value of approximately 0.4°C. The low difference between the inlet and outlet fluid temperature is attributed to the low thermal conductivity of the dry sand (0.289 W/(mK)). The inlet fluid temperature was then used as the input data, while the outlet fluid temperature was used to verify the outlet fluid temperature obtained from the numerical model results.

Fig. 10 presents the fluid temperature profile on the outer surface along the CCU after TRT for 16 hours. The initial temperature of the water was recorded as 13°C. Following the 16-hour operation, the inlet fluid temperature reached 62.9°C, while the outlet temperature was 62.5°C, as shown in Fig. 9. Logically, the temperature at the first spiral on the outer surface of the CCU was expected to be the highest, as it is close to the heat source from the inlet fluid temperature. However, interestingly, the results showed that the second spiral coil has the highest temperature, reaching 55.5°C while the first spiral reached 55°C. This unexpected outcome can be explained by the fact that the first spiral has a larger space for heat dissipation leading to this phenomenon. Furthermore, due to limited space for heat dissipation, the second spiral experiences reduced heat dissipation, resulting in a higher temperature compared to the first spiral coil. The temperature along the CCU gradually decreased from the third spiral to the eighth spiral coil and reached 54.9°C, 54.6°C, 54.5°C, 54.3°C, 53.9°C, and 53.2°C, respectively.

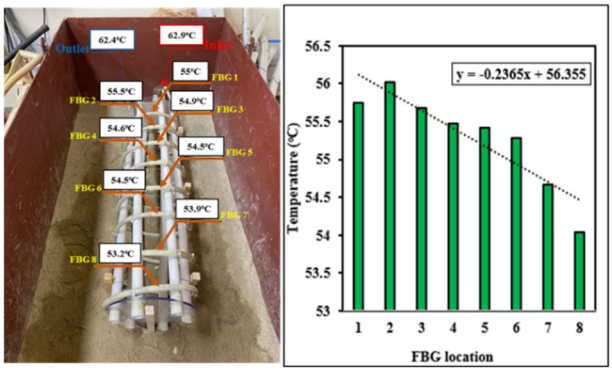

Fig. 10 Temperature changes every spiral of coil column unit

Fig. 11 Position of RTD sensor for measuring soil temperature distribution

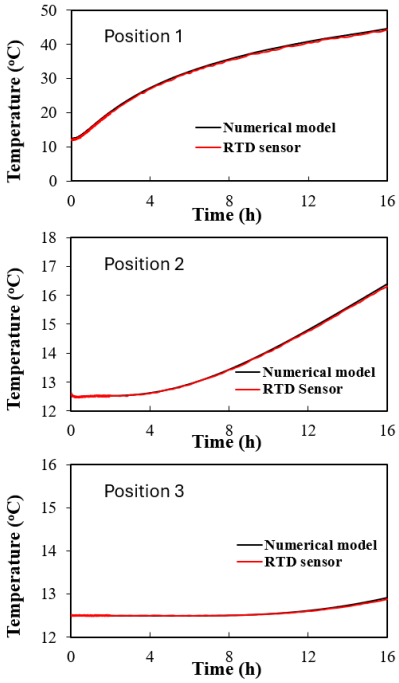

Fig. 12 Soil temperature distribution at three positions

5.3 Verification of numerical model for coil column unit

To validate the heat transfer in the solid of the numerical model (conduction heat) of the coil column unit, a comparison was conducted between the temperature of natural sand at three specified positions, as indicated in Fig. 11, obtained from both experiment and numerical analysis. The results of this comparison are presented in Fig. 12. In addition, the heat transfer of the fluid flow in the pipe (heat convection) was also validated by calculating and comparing the heat exchange of both TRT and numerical models using inlet and outlet fluid temperature data. The heat exchanger, Q, can be calculated as follows

$$Q = mc(T_{in} - T_{out}) \tag{16}$$

where Q is heat exchange (W), m is the flow rate of the fluid (kg/m), and T_{in} and T_{out} is the temperature of inlet and outlet fluid (°C), c is the specific heat capacity (J/kg. °C)

The verification between the numerical model and the experiment results is presented in Fig. 12 for heat conduction (temperature of sand) and Fig. 13 for heat convection (heat exchange calculated by the inlet and outlet fluid temperature). A very good agreement between the

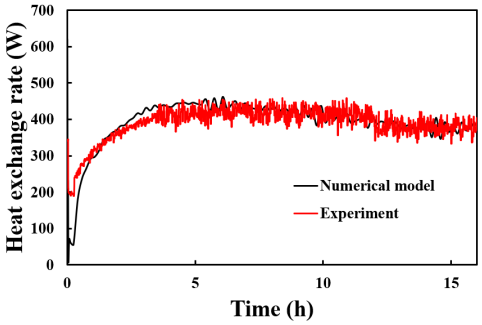

Fig. 13 Heat exchange rate comparison between numerical analysis and experiment of the coil column unit

numerical and experimental results for both heat conduction and heat convection demonstrates that the numerical model can be highly reliable and accurate for simulating the heat transfer process of the CCU as a heat exchanger of the geothermal system.

5.4 Temperature change comparison between numerical analysis and experimental measurements of the coil column unit

Fig. 14 presents the results of temperature measurement using FBG sensors and numerical analysis. The numerical model results agree well with the experimental results measured by FBG sensors. In detail, the temperature differences observed between the numerical and experimental models at each spiral were as follows: 0.307°C for the first spiral, 0.178°C for the second spiral, 0.452°C for the third spiral, 0.297°C for the fourth spiral, 0.287°C for the fifth spiral, 0.222°C for the sixth spiral, 0.292°C for the seventh spiral, and 0.095°C for the eighth spiral. From the results obtained above, the difference was found to be lower than 1%. Comparatively, when conventional sensors such as RTD sensors were employed, a temperature difference of approximately, 4% in the study of (Larwa and Kupiec 2020), or less than 5% (Li *et al.* 2012) for ground heat pump systems using the TRNSYS model was observed between the experimental and numerical models in previous studies. Therefore, the results obtained from FBG sensors demonstrated that the FBG sensors are accurate and reliable for measuring the temperature during the heat transfer process of the GSHP system. Consequently, the FBG sensor can effectively replace the conventional temperature sensors for temperature measurement applications within the GSHP system and its results can be used for validation of the heat transfer numerical model of CCU.

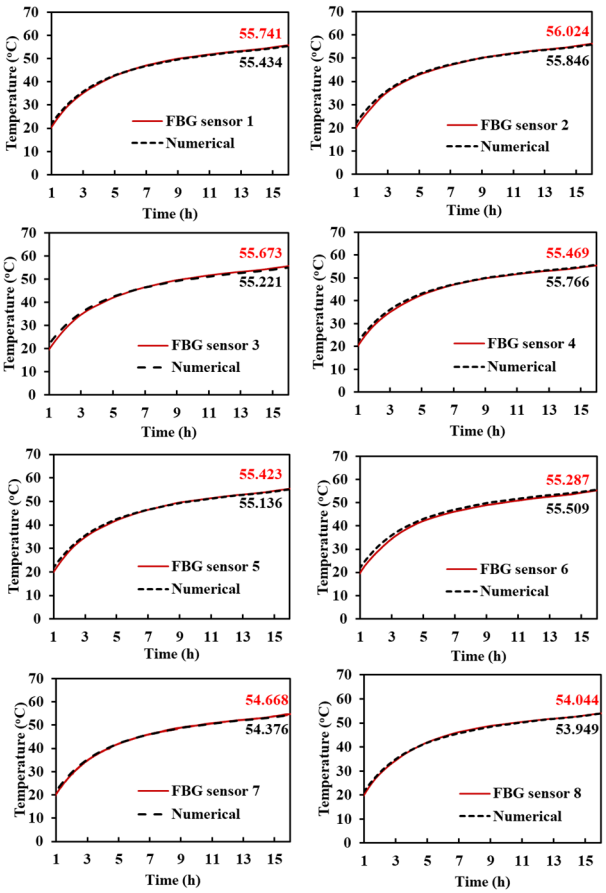

Fig. 14 Temperature change comparison between numerical analysis and experimental measurement of the coil column unit

6. Conclusions

This study proposed to use the FBG sensors to measure the temperature change during the heat transfer process of a ground heat exchanger of the geothermal energy system. The FBG sensors were calibrated with the conventional RTD sensor using a thermal chamber. The calibrated FBG sensors were then used to measure the temperature change during the thermal response test of the coil-column unit. Afterward, the numerical model based COMSOL Multiphysics was used to simulate the TRT and to verify the temperature measurement using the FBG sensors. The results indicated that the difference between the numerical results and the experiment results was lower than 1%. This result demonstrated that it is feasible to use the FBG sensor to record the change in the temperature during the test, supporting the validation of the numerical for future parametric studies, such as to determine the thermal properties of the soil or backfill material (back calculation) and design the configuration of the GHE of a geothermal energy system.

Acknowledgments

The research described in this paper was financially supported by the Basic Research Laboratory (BRL) research grant from the National Research Foundation of Korea (NRF) (No. 2022R1A4A1033838).

References

Bharathwaj, V., Markan, A., Atrey, M., Neumann, H. and Ramalingam, R. (2014), "Fiber Bragg Gratings for distributed cryogenic temperature measurement in a tube in tube helically coiled heat exchanger", In: *Sensors*, pp. 1535-1538. https://doi.org/10.1109/ICSENS.2014.6985308

Chen, Y., Mo, S., Li, W., Huang, L., Wen, S. and He, Z. (2023), "Applications of distributed fiber Bragg gratings to the measurements of in-tube fluid temperature distribution", *Appl. Thermal Eng.*, **220**, 119724. https://doi.org/10.1016/J.APPLTHERMALENG.2022.119724

Cheng-Yu, H., Yi-Fan, Z., Meng-Xi, Z., Lai, L., Gordon, M. and Li-Qiang, L. (2016), "Application of FBG sensors for geotechnical health monitoring, a review of sensor design, implementation methods and packaging techniques", *Sensors Actuat. A*, **244**, 184-197. https://doi.org/10.1016/j.sna.2016.04.033

Chong, C.S.A., Gan, G., Verhoef, A., Garcia, R.G. and Vidale, P.L. (2013), "Simulation of thermal performance of horizontal slinky-loop heat exchangers for ground source heat pumps", *Appl. Energy*, **104**, 603-610. https://doi.org/10.1016/j.apenergy.2012.11.069

Churchill, S.W. (1977), "Friction-factor equation spans all fluid-flow regimes", In: *Chemical Engineering*, New York, **84**, 91-92.

Congedo, P.M., Colangelo, G. and Starace, G. (2012), "CFD simulations of horizontal ground heat exchangers: A comparison among different configurations", *Appl. Thermal Eng.*, **33-34**, 24-32. https://doi.org/10.1016/j.applthermaleng.2011.09.005

Dinh, B.H., Kim, Y.S. and Kang, G.O. (2020), "Thermal conductivity of steelmaking slag-based controlled low-strength materials over entire range of degree of saturation: A study for ground source heat pump systems", *Geothermics*, **88**, 101910. https://doi.org/10.1016/j.geothermics.2020.101910

Dinh, B.H., Go, G.H. and Kim, Y.S. (2021), "Performance of a horizontal heat exchanger for ground heat pump system: Effects of groundwater level drop with soil–water thermal characteristics", *Appl. Thermal Eng.*, **195**, 117203. https://doi.org/10.1016/j.applthermaleng.2021.117203

Dinh, B.H., Kim, Y.S. and Yoon, S. (2022), "Experimental and numerical studies on the performance of horizontal U-type and spiral-coil-type ground heat exchangers considering economic aspects", *Renew. Energy*, **186**, 505-516. https://doi.org/10.1016/j.renene.2022.01.001

Dinh, H.B., Nguyen, C.H., Kim, H.K. and Kim, Y.S. (2023), "Consistency in thermal conductivity measured via lab-, field-scale test, and numerical simulation for newly developed backfill materials for underground power cable system", *Thermal Sci. Eng. Progress*, **46**, 102205. https://doi.org/10.1016/j.tsep.2023.102205

Jerez Lazo, C., Lee, N., Tripathi, P., Joykutty, L., Jayachandran, K. and Lee, S.J. (2024), "A fungus-based soil improvement using Rhizopus oryzae inoculum", *Int. J. Geo-Eng.*, **15**. https://doi.org/10.1186/s40703-024-00218-0

Jing, Z. and Yongqian, L. (2009), "Calibration method for fiber Bragg grating temperature sensor", *ICEMI 2009 - Proceedings of 9th International Conference on Electronic Measurement and Instruments*, pp. 2822-2825. https://doi.org/10.1109/ICEMI.2009.5274437

Kersey, A.D., Davis, M.A., Patrick, H.J., LeBlanc, M., Koo, K.P., Askins, C.G., Putnam, M.A. and Friebele, E.J. (1997), "Fiber grating sensors", *J. Lightwave Technol.*, **15**, 1442-1462. https://doi.org/10.1109/50.618377

Kim, H., Kang, D. and Kim, D.H. (2017), "Mechanical strength of FBG sensor exposed to cyclic thermal load for structural health monitoring", *Smart Struct. Syst.*, *Int. J.*, **19**(3), 335-340. https://doi.org/10.12989/sss.2017.19.3.335

Kim, Y.S., Dinh, B.H., Do, T.M. and Kang, G.O. (2020), "Development of thermally enhanced controlled low-strength material incorporating different types of steel-making slag for ground-source heat pump system", *Renewable Energy*, **150**, 116-127. https://doi.org/10.1016/j.renene.2019.12.129

Kim, Y.S., Dinh, H.B., Kang, G.O. and Hoang, D.T. (2023), "Performance evaluation of a novel horizontal ground heat exchanger: Coil-column system", *J. Build. Eng.*, **76**, p. 107180. https://doi.org/10.1016/j.jobe.2023.107180

Kumar, J., Prakash, O., Agrawal, S.K., Mahakud, R., Mokhariwale, A., Dixit, S.K. and Nakhe, S.V. (2016), "Distributed fiber Bragg grating sensor for multipoint temperature monitoring up to 500°C in high-electromagnetic interference environment", *Optical Eng.*, **55**(9), 090502-090502. https://doi.org/10.1117/1.OE.55.9.090502

Larwa, B. and Kupiec, K. (2020), "Determination of pipe wall temperature in a slinky-coil ground heat exchanger", *Int. J. Heat Mass Transfer*, **160**, p. 120202. https://doi.org/10.1016/j.ijheatmasstransfer.2020.120202

Lee, J.H., Kim, S.G., Park, H.J. and Song, M. (2006), "Investigation of Fiber Bragg grating temperature sensor for applications in electric power systems", *Proceedings of the IEEE International Conference on Properties and Applications of Dielectric Materials*, pp. 431-434. https://doi.org/10.1109/ICPADM.2006.284207

Li, H., Nagano, K. and Lai, Y. (2012), "A new model and solutions for a spiral heat exchanger and its experimental validation", *J. Heat Mass Transfer*, **55**(15-16), 4404-4414. https://doi.org/10.1016/j.ijheatmasstransfer.2012.03.084

Li, G., Feng, F., Wang, F. and Wei, B. (2022), "Temperature field measurement of photovoltaic module based on fiber Bragg grating sensor array", *Materials*, **15**(15), p. 5324. https://doi.org/10.3390/ma15155324

Marrah, M.Y., Fall, M. and Almansour, H. (2023), "Numerical simulation of ground thermal response in Canadian seasonal frost regions to climate warming", *Int. J. Geo-Eng.*, **14**(1), p. 16. https://doi.org/10.1186/s40703-023-00196-9

Montagud, C., Corberán, J.M. and Ruiz-Calvo, F. (2013), "Experimental and modeling analysis of a ground source heat pump system", *Appl. Energy*, **109**, 328-336. https://doi.org/10.1016/J.APENERGY.2012.11.025

Multiphysics, C. (2015), COMSOL Multiphysics®v. 5.3. COMSOL AB, Stockholm, Sweden.

Nations, U., n.d. Renewable energy – powering a safer future | United Nations.

Nguyen, A.D., Nguyen, V.T. and Kim, Y.S. (2023), "Finite element analysis on dynamic behavior of sheet pile quay wall dredged and improved seaside subsoil using cement deep mixing", *Int. J. Geo-Eng.*, **14**(1), p. 9. https://doi.org/10.1186/s40703-023-00186-x

Olabode, O.P. and San, L.H. (2023), "Analysis of soil electrical resistivity and hydraulic conductivity relationship for characterisation of lithology inducing slope instability in residual soil", *Int. J. Geo-Eng.*, **14**(1), p. 7. https://doi.org/10.1186/s40703-023-00184-z

Raab, S., Mangold, D. and Müller-Steinhagen, H. (2005), "Validation of a computer model for solar assisted district heating systems with seasonal hot water heat store", *Solar Energy*, **79**(5), 531-543. https://doi.org/10.1016/j.solener.2004.10.014

Ren, L., Li, H., Sun, L. and Li, D. (2004), "FBG sensors for on-line temperature measurements", In: *Smart Structures and Materials 2004*: *Sensors and Smart Structures Technologies for Civil*, *Mechanical*, *and Aerospace Systems*, Vol. 5391, pp. 94-99. https://doi.org/10.1117/12.538749

REN21 (2023), Renewables in Energy Demand [WWW Document]. Renewables 2023 Global Status Report Collection. URL https://www.ren21.net/gsr-2023/modules/energy_demand/ (accessed 3.24.24).

Shah, S.K., Aye, L. and Rismanchi, B. (2022), "Validations of a double U-tube borehole model and a seasonal solar thermal energy storage system model", *Renew. Energy*, **201**, 462-485. https://doi.org/10.1016/J.RENENE.2022.10.109

Talebinejad, I., Fischer, C. and Ansari, F. (2009), "Serially multiplexed FBG accelerometer for structural health monitoring of bridges", *Smart Struct. Syst.*, *Int. J.*, **5**(4), 345-355. https://doi.org/10.12989/sss.2009.5.4.345

Venkatesan, V.N. and Ramalingam, R. (2017), "Numerical and experimental investigation of FBG strain response at cryogenic temperatures", In: *IOP Conference Series*: *Materials Science and Engineering*, Vol. 171, No. 1, p. 012133. https://doi.org/10.1088/1757-899X/171/1/012133

Wang, L., Han, J. and Song, Y. (2014), "Fatigue performance monitoring of full-scale PPC beams by using the FBG sensors", *Smart Struct. Syst.*, *Int. J.*, **13**(6), 943-957. https://doi.org/10.12989/sss.2014.13.6.943

Werneck, M.M. (2013), "A guide to fiber bragg grating sensors, in current trends in shortand long period fiber gratings", IntechOpen 1-24.

Woo, H.J. and Go, G.H. (2024), "Mechanical behavior assessment of retaining wall structure due to frost heave of frozen ground", *Int. J. Geo-Eng.*, **15**(1), p. 7. https://doi.org/10.1186/s40703-024-00210-8

Wu, Y., Gan, G., Verhoef, A., Vidale, P.L. and Gonzalez, R.G. (2010), "Experimental measurement and numerical simulation of horizontal-coupled slinky ground source heat exchangers", *Appl. Thermal Eng.*, **30**, 2574-2583. https://doi.org/10.1016/j.applthermaleng.2010.07.008

Yang, W., Xu, R., Wang, F. and Chen, S. (2020), "Experimental and numerical investigations on the thermal performance of a horizontal spiral-coil ground heat exchanger", *Renew. Energy*, **147**, 979-995. https://doi.org/10.1016/j.renene.2019.09.030

Zhang, X., Liang, D., Zeng, J. and Lu, J. (2014), "SVR model reconstruction for the reliability of FBG sensor network based on the CFRP impact monitoring", *Smart Struct. Syst.*, *Int. J.*, **14**(2), 145-158. https://doi.org/10.12989/sss.2014.14.2.145